Springer

KSME

Journal of Mechanical Science and Technology 30 (2) (2016) 519~524
www.springerlink.com/content/1738-494x(Print)/1976-3824(Online)
DOI 10.1007/s12206-016-0104-y

Performance investigation of a counter-rotating tidal current turbine by CFD and model experimentation †

Nak Joong Lee[1], In Chul Kim[1], Beom Soo Hyun[2] and Young Ho Lee[3,*]

[1]*Graduate School Department of Mechanical Engineering, Korea Maritime & Ocean University, Busan, 606-791, Korea*
[2]*Division of Naval Architecture and Ocean System Engineering, Korea Maritime & Ocean University, Busan, 606-791, Korea*
[3]*Division of Mechanical Engineering, Korea Maritime & Ocean University, Busan, 606-791, Korea*

(Manuscript Received June 6, 2015; Revised August 26, 2015; Accepted September 15, 2015)

Abstract

Global warming is one of the issues in the world, which is mainly due to the burning of fossil fuels. Thus, alternative energy is now paramount in the 21st century. In Korea, the tidal currents in the southwestern sea have a wide range of currents that are available for tidal current power generation. Single rotor turbines can obtain a theoretical maximum power coefficient of 59.3%, whereas dual rotor turbines can attain a maximum of 64%. In this study, the performance and efficiency of a counter-rotating tidal current turbine is investigated when changing the front and rear blade angles at different water velocities. The investigation was conducted by using Computational fluid dynamics (CFD) and experimental methods highlighted in this study. When varying these parameters, changes in the streamlines were observed in the CFD results. The changes in flow stability over the blade surfaces observed in the numerical results were reflected in the power and power coefficient graphs presented in this study. The results obtained by the experiments were also shown to be in good agreement with the CFD results.

Keywords: Blade angle; Counter-rotating; Tidal current turbine; CFD; Wave tank experiment

1. Introduction

In recent times, various countries are looking to increase the use of renewable energy. One of the different sources of energy is the ocean, wherein the sun's energy is converted into several natural phenomena, such as tides and waves. Ocean energy conversion devices fall into two main categories, namely, wave and tidal energy conversion.

The oceans around Korea, the southwestern sea in particular, have tidal currents with a potential for tidal current power generation. Kim et al. [1] summarized a number of studies that has been conducted to investigate the feasibility of the tidal range and tidal current energy in Korea.

The main advantage of tidal power generation is that it is predictable and it is a reliable energy source because it does not rely on the weather or seasons. The kinetic energy within a tidal current can be converted into a usable form of energy by utilizing a Marine current turbine (MCT). The surrounding marine environment is not significantly disturbed as seawater is still able to flow naturally through the MCT as it produces power from water velocity. Currently, the most advanced and economically feasible MCT is the horizontal-axis-type MCT [2]. Its operating principle is similar to horizontal axis wind turbines, and the advances made in the wind industry have also been reflected in the development of this type of turbine.

According to the Betz theorem, single rotor turbines are calculated to have a theoretical maximum efficiency of 59.3%, whereas dual rotor turbines can obtain a maximum of 64% [3]. Therefore, with an additional rotor revolving in the opposite direction, the turbine can extract more kinetic energy from the flow. Thus, by optimizing a counter-rotating turbine, more power can be obtained by a dual rotor turbine than a single rotor turbine at the same current speed.

A 40 W counter-rotating model horizontal-axis-type MCT was designed for experiments according to Blade element momentum theory (BEMT). The BEMT uses a combination of momentum theory equations and blade element theory [4]. Prandtl's tip loss factor was also accounted for on the basis of the discrete number of blades. Yang [5] assessed the optimization of a 100 kW horizontal-axis-type MCT that was designed by BEMT with the addition of Prandtl's tip loss factor. Batten et al. [6] used a numerical program based on BEMT to predict the performance of an MCT and compared it to the test results from the cavitation tunnel experiments for validation. The results were in good agreement; thus, the optimization of the design, as well as other designs, was possible.

*Corresponding author. Tel.: +82 51 410 4293, Fax.: +82 51 403 1214
E-mail address: lyh@kmou.ac.kr
† This paper was presented at the ISFMFE 2014, Wuhan, China, October 2014.
Recommended by Guest Editor Hyung Hee Cho and Yulin Wu

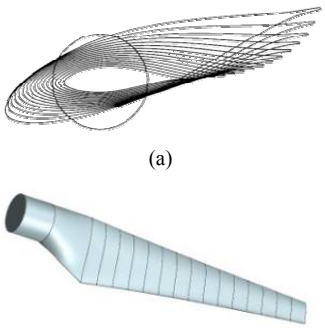

(a) (b)

Fig. 1. (a) View of the blade from the tip, which shows the different chord lengths and twist angles; (b) 3D model of the turbine rotor.

This model turbine is used for small-scale experimental tests to analyze the performance characteristics. The turbine is planned to be scaled up to a size that can produce 10 kW within a submerged floating structure.

Previous experiments on this model focused on the effect of varying the distance between the front and rear blades on the power characteristics of the turbine. This study will be investigating the effect of changing the front and rear blade angles on the performance of the turbine.

Along with the experimental results, the turbine setup and the experimental conditions will be simulated by using a commercial Computational fluid dynamics (CFD) software. Kim et al. [7] evaluated the performance of a 100 kW MCT using a finite volume-based commercial solver, ANSYS CFX, and investigated the three-dimensional (3D) flow characteristics and blade surface streamlines. The results from both investigations will be compared and further discussed in this study.

2. Numerical procedure

For this study, the 40 W MCT model has three blades per rotor, with each rotor designed by BEMT. The diameter (D) of the turbine was 500 mm, and the design water speed was 1 m/s. The design rotational speed is 190 rpm. The distance between the rotors was 250 mm. This specific distance was the subject of a previous study [8] on the current turbine blade design.

Fig. 1 shows the two-dimensional and 3D models of turbine blade design. The top figure shows the blade seen from its tip. Different chord lengths and blade twist angles, which were calculated using BEMT, can be observed. The bottom figure presents the 3D model of the rotor. The lines show the location of sections where the chord length and twist angles were specified during modeling.

Fig. 2 shows the computational mesh of the hexahedral elements of the domain and blade. The top figure shows the mesh of the entire domain with only one blade per rotor meshed. The remaining blades were accounted for by periodic conditions. The distance from the blades to the inlet, top, and

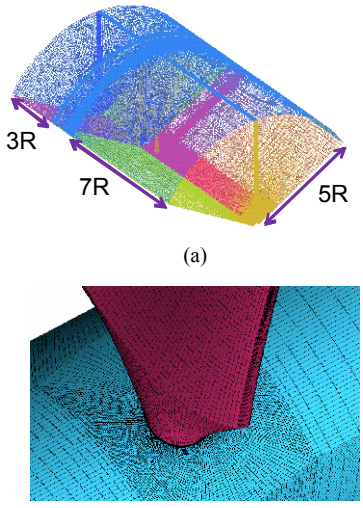

(a) (b)

Fig. 2. (a) Computational mesh of the domain; (b) grid distribution near the blade and hub.

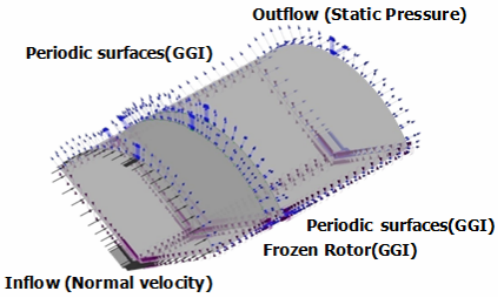

Fig. 3. Computational domain of the rotor blade.

outlet was three, five, and seven times the diameter of the blade, respectively. The grid distribution near the blade is shown at the bottom of Fig. 2. The mesh was refined near the wall of the blade. The non-dimensional distance of the first node from the wall or the y-plus value was less than five in this calculation, with approximately 6.2 million nodes in the hexa-grid. This value of y-plus is important to calculate the turbulence near the wall boundary accurately [9].

Fig. 3 shows the computational domain and boundary conditions that were set in CFX-Pre, a pre-processing software. The turbulence model used was k–ω SST. This model was selected because it can accurately model the turbulent shear stress and the amount and onset of flow separation under adverse pressure gradients [9]. All calculations were conducted under a steady-state condition using a commercial finite volume method solver, ANSYS CFX ver.13. The water velocity was varied from 0.8 m/s to 2.0 m/s and was specified in the inlet labeled “Inflow” in Fig. 3. At the outlet labeled “Outflow,” an opening boundary condition with static pressure was specified. A frozen rotor condition was set for the domain of the turbine, and the rotational speed of the turbine was specified at 190 rpm.

Fig. 4. Circulating water channel.

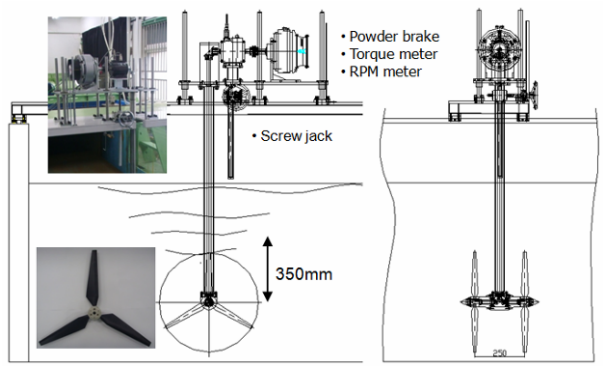

Fig. 5. Schematic of the experimental setup. The center of the turbine is located 350 mm below the free surface.

3. Experimental procedure

The experiments were conducted in a water tank with a vertically circulating water channel located within the Korea Maritime and Ocean University (KMOU). The height of the tank is 1200 mm, the width is 1800 mm, and the length is 4000 mm. The height of the water level used for this experiment was 900 mm.

Fig. 4 shows the water channel, turbine, control panel for the channel, and two fans used to regulate the water velocity in the water channel.

Fig. 5 shows a schematic of the experimental setup and the location of the turbine below the free surface. The center of the turbine is located approximately 350 mm below the surface of the water. The powder brake, torque transducer, and rpm sensor were attached to the turbine setup for measurement, and the data were recorded in the data logger. The torque meter (model SBB) had a measurement range from 0 kgf-m to 2 kgf-m. The torque meter contained an rpm sensor (MP-981) with a measurement range of up to 10000 rpm. A forced air-cooled-type powder brake (PRB-5Y3F model) was used to control the rpm of the turbine. The blockage ratio of the system was 12%. Therefore, a blockage correction factor was applied to the results [10, 11]. Experiments were conducted by varying the water flow from 0.6 m/s to 1.3 m/s. The Pitot tube was kept at 1 m in front of the turbine and measured

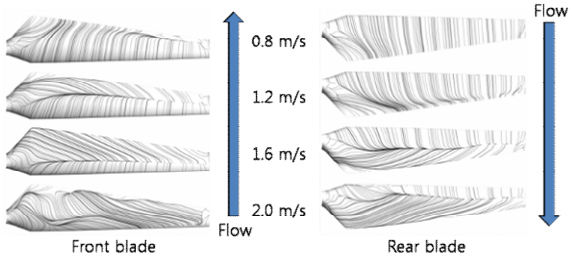

Fig. 6. Suction side surface streamlines ($F = 0°$, $R = -5°$).

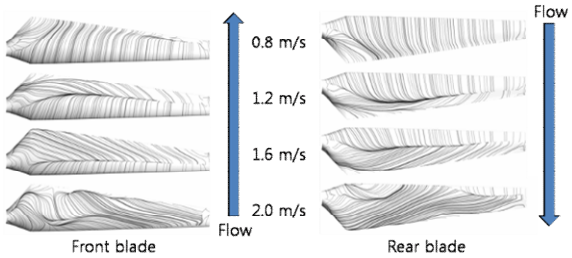

Fig. 7. Suction side surface streamlines ($F = 0°$, $R = 0°$).

the water velocity. In the same manner as the numerical case, the distance between the dual rotors was fixed at 250 mm.

The blades of the turbine were made of aluminum, and each blade was fabricated from a single piece using a five-axis milling machine. The total number of blades made was six.

4. Results

Fig. 6 depicts the streamlines observed at the suction side of the front and rear blades at a water velocity of 0.8–2.0 m/s, in which the arrows indicate the direction of the flow. The arrangement is such that the front blade (F) is positioned at 0° and the rear blade (R) is at −5°. Both blades show a stable flow over the blade surface with little to no turbulent flow at lower velocities. However, as the flow velocity increases, the flow becomes less likely to remain stable on the surface. Flow separation can be observed on the front blade from 1.2 m/s to 2.0 m/s. The nature of the streamlines indicates that the flow at the rear blade does not separate to the extent as that in the front blade because of the reduction of velocity in the wake of the front blade. Fig. 7 shows the suction side streamlines for front and rear blades both fixed at 0° to the flow obtained from CFD calculations. The flow remains stable below the design speed of 1 m/s in a similar pattern, as shown in Fig. 6. As the water velocity increases, the flow also becomes more turbulent over the surface of both blades. The flow was observed to be more turbulent on the rear blade than the previous one at 2.0 m/s. Fig. 8 shows the streamlines from the CFD calculations when the rear blade was angled at 5° to the flow, whereas the front blade was fixed at 0°. The flow pattern over the front blade surface shows that it was quite similar to the previous cases (Figs. 6 and 7). However, the rear blade exhibits an increase in turbulent flow occurrence for all water velocities. Figs. 9 and 10 show the surface streamline cases

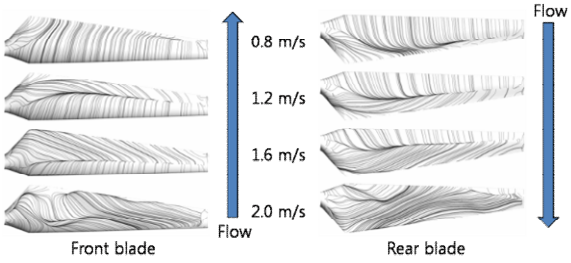

Fig. 8. Suction side surface streamlines ($F = 0°$, $R = 5°$).

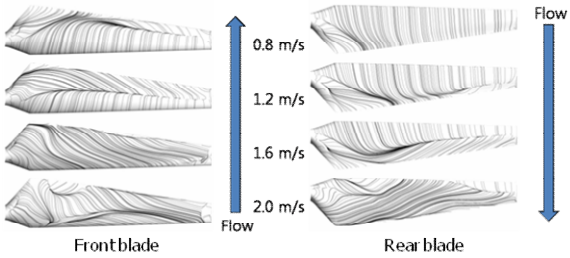

Fig. 9. Suction side surface streamlines (F = −5°, $R = 0°$).

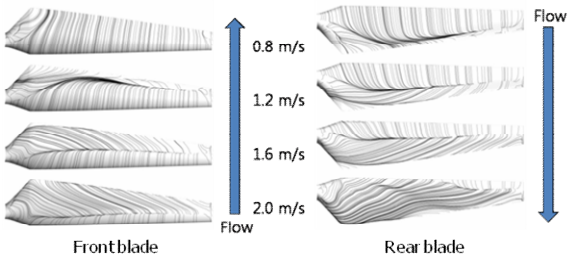

Fig. 10. Suction side surface streamlines ($F = 5°$, $R = 0°$).

when the rear blade is fixed at 0°. Fig. 9 illustrates the streamlines when the front blade is at −5° to the incoming flow. At a water velocity of 0.8 m/s, a relatively lesser amount of turbulent flow was observed on both blades. However, as the velocity increases, the flow begins to separate on the front blade much earlier than the rear. The flow on the rear blade does not fully become turbulent until 2 m/s. Fig. 10 shows the surface flow on the blades when the front blade is angled at 5°. In this case, the flow on the front blade does not completely separate at higher velocities and the streamlines show that most of the flow stay on the blade at lower velocities. However, the rear blade streamlines are similar to the previous cases.

Fig. 11 shows the comparison between the power output developed during the experiments and the power output obtained by CFD calculations at varied water velocities with the front blade fixed at 0° and varied rear blade angle. The limitation of the experimental setup is its inability to produce water velocities larger than 1.4 m/s. However, velocities over this speed caused a considerable number of problems, such as a sudden stoppage in the operation of the water channel during experimentation. The trends of the graph show that the experimental and CFD results are in good agreement over all velocities. The

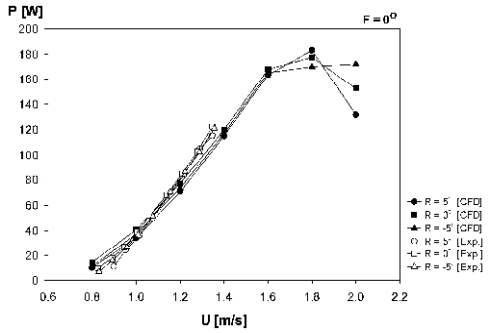

Fig. 11. Comparison of the power characteristics between experiments and CFD when $F = 0°$ and rear blade (R) angle is varied.

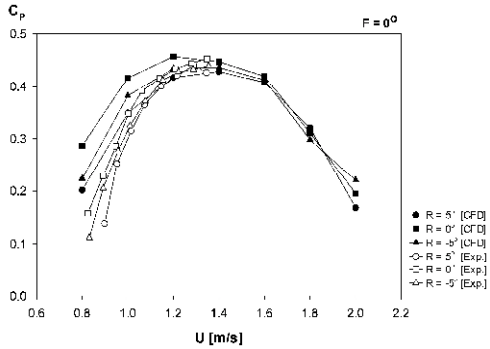

Fig. 12. Comparison of the power coefficients between CFD and experiments when $F = 0°$ and rear blade (R) angle is varied.

experimental results showed slightly lower power from 0.8 m/s to 1.1 m/s but slightly higher power at velocities over this range. The difference between the produced powers was observed to be little when the rear blade angles were changed, except at 2.0 m/s. The maximum power obtained from CFD was approximately 183 W at 1.8 m/s when the rear blade angle was positioned at 5°.

The comparison between the power coefficients (Cp) obtained from CFD calculations and the experimental result at a fixed front blade angle is presented in Fig. 12. The nature of the graph indicates that the Cp obtained from experimental data is lower than that of the CFD results. The difference between the power coefficients can be easily noticed in the graph as the rear angle is altered. For the experiments and CFD calculations, high Cp is obtained as the front and rear angles are positioned at 0° to the flow. The trend clearly shows an increase in Cp as the water velocities increase until a maximum is reached at approximately 1.2–1.4 m/s and then decrease until 2.0 m/s. The highest Cp value of 0.457 was obtained at 1.2 m/s from CFD, whereas highest Cp value of 0.453 was obtained at a 1.4 m/s water velocity from the experiments.

Fig. 13 shows the power output comparison of the turbine between the CFD and experimental results when the front blade angle is varied and when the rear blade angle is fixed at 0°. Each case presented in this figure shows the increase in power output as the velocity increases until approximately 1.4

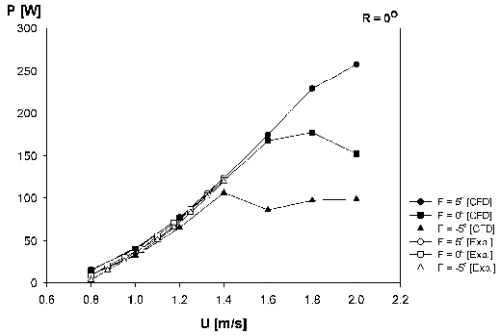

Fig. 13. Comparison of the power characteristics between experiments and CFD when $R = 0°$ and front blade (F) angle is varied.

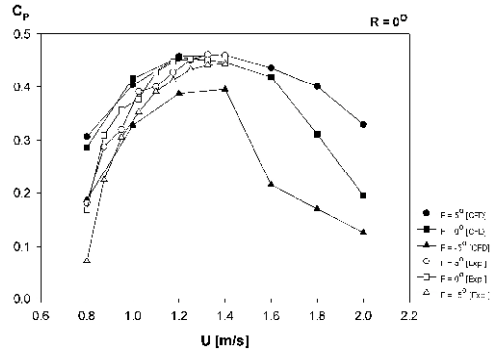

Fig. 14. Comparison of the power coefficients between experiments and CFD when $R = 0°$ and front blade (F) angle is varied.

m/s before decreasing until 2 m/s. This decrease accounts for the loss of flow stability on the front blade, as shown by the streamlines. The graph shows the close agreement between the CFD and experimental results. As the experiments were conducted up to the water velocity of 1.4 m/s, only the CFD data are plotted above the said velocity. The power output obtained is 123.514 and 123.405 W from the CFD and experiments at 1.4 m/s, respectively, when the front blade is angled at 5° and the value being almost equal. The maximum power attained is 258 W at a 2 m/s water velocity for the front angle at 5°.

Fig. 14 shows the plot of *Cp* versus the water velocity as the rear blade is fixed. The graph obtained when the front blade is angled at 5° shows higher values of *Cp* as compared with other cases. For this case, the maximum *Cp* obtained from the CFD and experiments is 0.460 at 1.4 m/s and 0.461 at 1.302 m/s water velocity, respectively. When both blade angles are fixed at 0°, the maximum *Cp* acquired is 0.457 at 1.2 m/s for the CFD case and 0.461 at 1.302 m/s for the experimental case. By contrast, when the blade is angled at −5°, the values of *Cp* is lower as compared with the other two cases in which the maximum *Cp* attained is 0.395 at 1.4 m/s for the CFD case and 0.445 at 1.372 m/s for the experimental case. The highest power output obtained during the experiment is 123.405 W for a 1.372 m/s water velocity.

5. Conclusions

A CFD analysis was conducted to determine the effects of blade angle changes on the performance characteristics of the tidal current turbine. Experiments were conducted in the water tank with a vertically circulating water channel at KMOU to validate the numerical results. Streamlines provided the flow pattern over the front and rear blades at various water velocities when the front blade angle is fixed, whereas the rear blade angle is varied from −5° to 5° and vice versa. The pattern indicates that, as the rear blade angle increases, the more turbulent the flow becomes. The trends of the graph show that the experimental and CFD results are in good agreement over all velocities. When the front blade was fixed, the experimental results showed a slightly lower power from 0.8 m/s to 1.1 m/s but a slightly higher power at velocities over this range. When the rear blade angle was fixed and the front blade was varied, the 5° front blade angle showed better flow stability on the surface. The power outputs produced and the power coefficients obtained were also presented for the aforementioned cases. The power output from the CFD and experiments when the front blade was fixed was 115 W at 1.4 m/s with a maximum *Cp* of 0.46 and 115.17 W with a maximum *Cp* of 0.45, respectively. Similarly, when the rear blade was fixed, the power output from the CFD and experiments was 123.5 W at 1.4 m/s and 123.41 W at 1.37 m/s, respectively, with a maximum *Cp* of 0.46 for both.

Acknowledgments

This work was supported by the New & Renewable Energy Core Technology Program of the Korea Institute of Energy Technology Evaluation and Planning and was granted financial resource from the Ministry of Trade, Industry, & Energy, Republic of Korea. (20133030000260).

References

[1] G. W. Kim, M. E. Lee, K. S. Lee, J. S. Park, W. M. Jeong, S. K. Kang, J. G. Soh and H. Kim, An overview of ocean renewable energy resources in Korea, *Renewable and Sustainable Energy Reviews*, 16 (2012) 2278-2288.

[2] K. W. Ng, W. H. Lam and K. C. Ng, 2002-2012: 10 Years of research progress in horizontal-axis marine current turbines, *Energies*, 6 (2013) 1497-1526.

[3] B. G. Newman, Multiple actuator-disc theory for wind turbines, *Journal of Wind engineering and Industrial Aerodynamics*, 24 (1986) 215-225.

[4] J. F. Manwell, J. G. McGowan and A. L. Rogers, *Wind energy explained: theory, design and application*, Wiley and Sons, England (2002) 111-113.

[5] C. J. Yang, Optimal rotor blade design for tidal in-stream energy, *Journal of the Korean society of Marine Environment & Safety*, 17 (1) (2011) 75-82.

[6] W. M. J. Batten, A. S. Bahaj and A. F. Molland, J. R. Chap-

lin and sustainable energy research group, *Ocean Engineering,* 34 (2007) 1013-1020.

[7] B. G. Kim, C. J. Yang and M. S. Choi, A study on the performance of an 100 kW class tidal current turbine, *Journal of the Korean Society of Marine Environment & Safety*, 18 (2) (2012) 145-152.

[8] N. J. Lee, I. C. Kim, C. G. Kim, B. S. Hyun and Y. H. Lee, Performance study on a counter-rotating tidal current turbine by CFD and model experimentation, *Renewable Energy*, 79 (2015) 122-126.

[9] *ANSYS CFX. Solver modeling guide*, ANSYS Inc. (2009) 113-119.

[10] A. S. Bahaj, A. F. Molland, J. R. Chaplin and W. M. J. Batten, Power and thrust measurements of marine current turbines under various hydrodynamic flow conditions in a cavitation tunnel and a towing tank, *Renewable Energy*, 32 (2007) 407-426.

[11] T. Y. Chen and L. R. Liou, Blockage corrections in wind tunnel tests of small horizontal axis wind turbines, *Experimental Thermal and Fluid Science*, 35 (2011) 565-589.

Nak Joong Lee is currently undergoing his Ph.D. in Tidal Energy in the Korea Maritime and Ocean University. He completed his Bachelor's Degree in Engineering in 2009 and his Master's Degree in Engineering in 2012. His research interests include small hydropower, fluid machinery and computational fluid dynamics.

Young Ho Lee is currently a professor in the Division of Mechanical and Energy Systems at the Korea Maritime and Ocean University. He completed his Ph.D. in Engineering in Tokyo. His research interests include particle imaging velocimetry, renewable energy, fluid machinery, and computational fluid dynamics.